Behavior of Extraframework Fe Sites in MFI and MCM-22 Zeolites upon Interaction with N_2O and NO

Gloria Berlier,*,† Carmelo Prestipino,*,† Mickaël Rivallan,†,‡ Silvia Bordiga,† Carlo Lamberti,† and Adriano Zecchina†

Department of Inorganic, Physical and Materials Chemistry, and INSTM Research Unity of Turin University, NIS Center of Excellence, University of Torino, via P. Giuria, 7 I-10125 Torino, Italy, and LCISM, UMR6511, Institute of Chemistry, University of Rennes 1, F-35042 Rennes Cedex, France

Received: April 28, 2005; In Final Form: September 6, 2005

We report on the characterization of an isomorphously substituted Fe-MCM-22 sample containing both Fe and Al in framework positions (Si/Fe = 44, Si/Al = 25). XANES spectroscopy was used to study the evolution of Fe sites as a consequence of thermal activation at high temperature (1073 K) and subsequent oxidation with N_2O. The results were compared to those obtained in the same conditions on a well-known Fe-silicalite sample (Si/Fe = 68, Si/Al = ∞). In both samples, thermal activation causes migration of a fraction of Fe ions from framework to extraframework positions, this migration being accompanied by a reduction of Fe^{3+} to Fe^{2+}. Upon oxidation with N_2O at 523 K, the two samples show a different behavior. While in Fe-silicalite practically all of the Fe^{2+} sites formed by thermal activation are reoxidized to Fe^{3+}, in Fe-MCM-22 only a fraction of the extraframework iron sites is involved in the reoxidation process. The accessibility of the extraframework Fe sites was also investigated by using the NO molecule as a surface probe. Upon NO dosage on the sample, the modification of the pre-edge peak and of the edge position suggests an important charge release from the extraframework Fe^{2+} ions to the adsorbed molecules. This could be formalized with the formation of $Fe^{3+}(NO^-)$ complexes, compatible (on the basis of the simple molecular orbital theory) with a bent NO geometry. The formation of a complex family of Fe^{2+} mono-, di-, and trinitrosyl complexes was also confirmed by FTIR spectroscopy. Similarly to what was observed in the oxidation experiments, the fraction of extraframework Fe sites able to interact with NO in Fe-MCM-22 sample is smaller than that in Fe-silicalite treated in the same conditions. This trend is explained with a major clustering of extraframework Fe sites in Fe-MCM-22 sample, as was also suggested by FTIR experiments. These results suggest that the dispersion of iron in zeolitic matrixes prepared by isomorphous substitution could also depend on the zeolitic structure.

1. Introduction

Because of the redox properties of iron, which can show different valence states (Fe^{2+}, Fe^{3+}, and even Fe^{4+}), Fe-containing zeolites have been the subject of extensive studies since the 1970s.[1] Initially, people have tried to insert iron by post synthesis methods inside the channels and cavities of different zeolitic structures, such as Y, Mordenite, and MFI.[2] Later, framework substituted Fe-MFI zeolites were synthesized[3,4] and deeply studied for their catalytic activity in the hydroxylation of benzene to phenol with nitrous oxide.[5] Moreover, Fe-zeolites also showed good activity and stability in the selective reduction (SCR) of nitric oxide with hydrocarbons[6,7] and ammonia.[8] The use of Fe-MFI for simple N_2O decomposition has also currently been investigated.[9−14]

An impressive number of papers were devoted to the investigation of Fe-MFI systems, debating the nature of the active sites in partial oxidation reactions. In particular, the main open questions regarded the nuclearity of active Fe species (isolated, dimeric, or clustered)[15−30] and the role of Al on their nature and activity.[16,31−37] The nature and distribution of Fe ions dispersed inside the zeolitic channels (extraframework species) were found to be highly sensitive upon the preparation method, the activation procedures, and the amount of introduced iron.[26,38] In particular, the formation of small oxidic clusters[20,38] and/or binuclear hydroxo-iron clusters[16,24,28−30] was observed at high iron loading, especially when postsynthesis methods were used. Conversely, Al-containing Fe-ZSM-5 samples with low iron loading, and thus highly active in selective oxidation reactions,[31] showed the main presence of isolated extraframework Fe^{2+} species, mostly located in the vicinity of framework Al species.[17,32,35−37]

Recently, the influence of the zeolitic structure on the nature, distribution, and activity of extraframework Fe ions has been examined by different authors.[12,25,39−50] In particular, Fe-containing Beta,[12,39−43] Ferrierite,[12,40,44,45] Mordenite,[40,46] and mesoporous MCM-41[25,47−50] are the most studied. Minor attention has been devoted to Fe-containing MCM-22[51−56] (MWW framework),[57,58] notwithstanding the fact that a considerably high amount of iron could be introduced in the T sites of its framework.

In this paper, an Al-containing Fe-MCM-22 sample, prepared by isomorphous insertion, is investigated by means of XANES and FTIR spectroscopies. The evolution of Fe ions as a

* Corresponding authors. C.P.: telephone, +39011-6707841; fax, +39011-6707855; e-mail, carmelo.pestipino@unito.it. G.B.: telephone, +39011-6707856; fax, +39011-6707855; e-mail, gloria.berlier@unito.it.

† University of Torino.

‡ University of Rennes.

10.1021/jp052210+ CCC: $30.25
Published on Web 11/08/2005

consequence of thermal activation, oxidation with N_2O, and dosing of NO was followed by high-resolution XANES. The results were compared to those obtained in similar conditions on a "classical" Al-free Fe-silicalite sample, showing a markedly different behavior of the extraframework Fe ions. We anticipate that our results show an opposite trend with respect to those recently reported by Hensen et al.,[34] indicating that the effect of Al on the structure of extraframework Fe species could be also sensitive to the zeolitic structure.

2. Experimental Section

The Fe-MCM-22 catalyst (Si/Fe = 44, Si/Al = 25) was prepared by the Aiello group (University of Calabria, I) following the method described in detail in ref 52. Fe-silicalite sample (Si/Fe = 68) was prepared in the laboratories of Prof. L. Forni (Dipartimento di Chimica Fisica ed Elettrochimica, Università di Milano) following the method described by Ratnasamy and Kumar.[59] After the synthesis, the catalysts were washed, dried, and calcined in nitrogen and then dry air at 823 K. Before each experiment, the catalysts were activated in a vacuum at 1073 K.

X-ray absorption experiments were performed at the GILDA BM8 beamline[60] at the European Synchrotron Radiation Facility (ESRF). The monochromator was equipped with two Si(311) crystals, and harmonic rejection was obtained by using a pair of flat, Pt-coated mirrors working at 10 mrad. To ensure high-quality XANES spectra, the geometry of the beamline was optimized to improve the energy resolution: vertical slits, located at 23 m from the source, were set to 0.6 mm, ensuring at 7 keV an actual energy resolution better than 0.4 eV. The following experimental geometry was adopted: (1) I_0 (1 bar N_2 filled ionization detector having efficiency of 10%); (2) zeolite sample; (3) I_1 (100 mbar Ar filled ionization detector having efficiency of 50%); (4) 3 μm thick iron metal foil; and (5) I_2 (photodetector).[61] This setup allows a direct energy/angle calibration for each spectrum, avoiding any problem related to little energy shifts due to small thermal instability of the monochromator crystals. A sampling step of 0.2 eV for the XANES part of the spectra and a variable sampling step, giving $\Delta k_{max} = 0.05$ Å^{-1} for the EXAFS part, and an integration time of 3 s/point have been adopted. Spectra were collected at room temperature using a metallic cell allowing in-situ high-temperature treatments and gas dosage, described in detail elsewhere.[62]

The IR experiments were carried out on a Bruker IFS 66 FTIR instrument equipped with a cryogenic MCT detector and running at 2 cm^{-1} resolution. Suitable measurement cells were used allowing in situ thermal treatments and dosing of NO. NO, carefully purified by distillation, was initially dosed at room temperature (P_{NO} = 15 Torr); the equilibrium pressure was reduced step by step, thus allowing us to obtain a sequence of IR spectra corresponding to decreasing NO coverage. The first spectrum collected just before the initial gas dosage was used as reference for obtaining the background-subtracted spectra. The intensity of the NO spectra was "normalized" in terms of the Fe content and of the thickness of the zeolite pellet, carefully weighted before the measurement.[33] The most diluted sample was chosen as a reference, that is, with a "normalization factor" of 1. The intensity of the bands obtained on the other sample was divided by a "normalization factor" corresponding to the amount of iron content crossed by the IR beam.

3. Results

3.1. XANES Spectroscopy on Fe-Silicalite. In Figure 1, the XANES spectra obtained upon activation at 1073 K (full line) and subsequent oxidation with N_2O at 523 K (dotted line) of the Fe-silicalite samples are reported. For comparison, the spectrum of the sample in the presence of the template, before any activation, is also reported (dashed line). The spectrum of the sample with template is characterized by a sharp and well-defined pre-edge peak at 7114.2 eV, assigned to the 1s → 3d transition ascribed to isolated Fe^{3+} species in tetrahedral framework positions. The peak is dramatically affected by the activation in vacuo at 1073 K; in fact, its intensity is halved passing from 0.16 to 0.08, and a well-defined second component appears at 7112.3 eV. This transformation is accompanied by a remarkable shift of the edge position, passing from 7124.1 to 7120.3 eV (position defined at half-height of the edge jump). After oxidation with N_2O at 523 K (dotted curve in Figure 1), the XANES edge position is back-shifted to high energy, resulting at 7124.1 eV. This is accompanied by the disappearance of the component at 7112.3 eV (see inset) and by the formation of a component at higher energy (7114.3 eV).

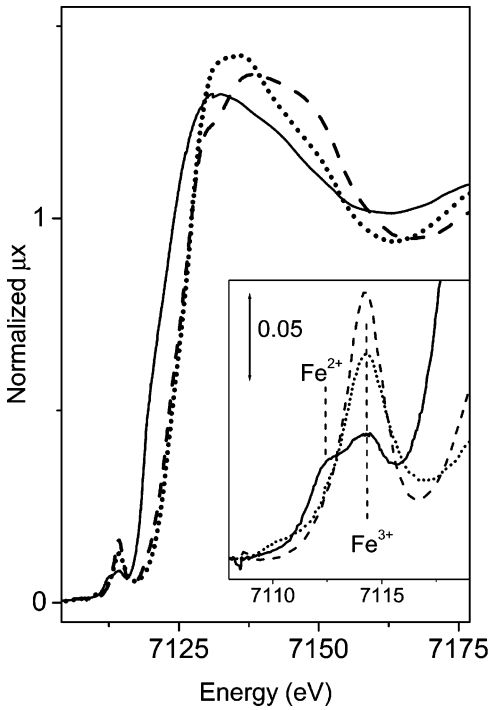

Figure 1. XANES spectra of sample Fe-silicalite with template (dashed line), after removal of template and subsequent activation at 1073 K (full line), and subsequent oxidation with N_2O at 523 K (dotted line). The inset shows the magnification of the pre-edge peaks.

Figure 2 shows the k^3-weighted Fourier transform of the EXAFS spectra obtained on Fe-silicalite in the same experiments discussed above. As commonly observed, the EXAFS spectra of well-prepared, template containing Fe-silicalite are characterized by the presence of a single peak corresponding to the first Fe−O shell, which is here found in the 0.8−2.24 Å range with a maximum at 1.5 Å. Thermal activation at 1073 K of Fe-silicalite causes a strong decrease of the intensity of the first Fe−O shell (compare full and dashed lines). Upon oxidation, the intensity of the first shell peak increases, indicating an increase in the average Fe order and coordination number.

The interaction between Fe sites in activated Fe-silicalite and NO molecules has been investigated by XANES spectroscopy, as shown in Figure 3 (dotted spectrum). The dosage of NO on the Fe-silicalite sample previously activated at 1073 K (full line spectrum) causes a deep modification of the XANES spectrum. From a superficial point of view, this change is roughly similar to that observed after oxidation with N_2O. In particular, a definite

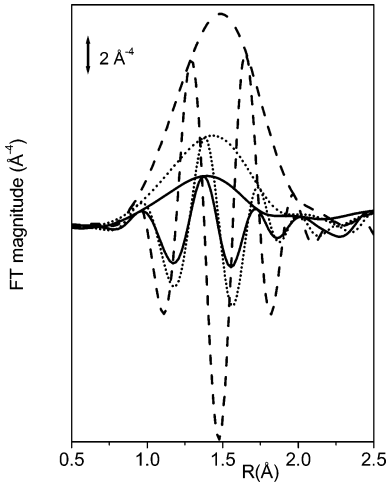

Figure 2. κ^3-weighted, phase uncorrected FT (modulus and imaginary parts) of sample Fe-silicalite with template (dashed line), after removal of template and subsequent activation at 1073 K (full line), and subsequent oxidation with N_2O at 523 K (dotted line).

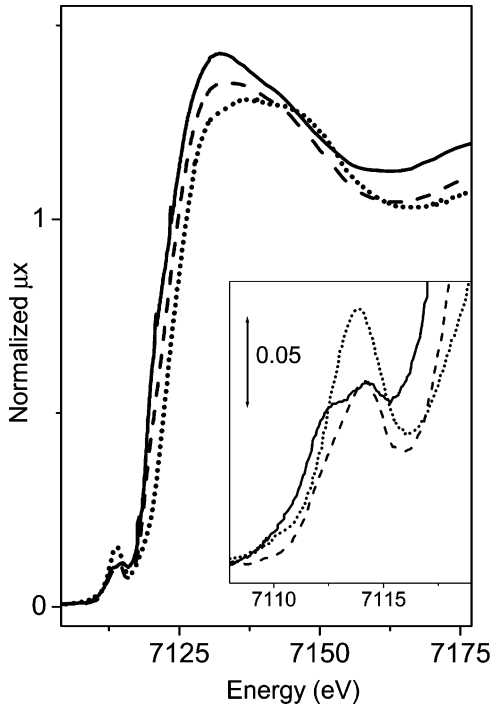

Figure 3. XANES spectra of sample Fe-silicalite after activation at 1073 K (full line), after dosage of 20 Torr NO at room temperature (dotted line), and subsequent outgassing at 573 K (dashed line). The inset shows the magnification of the pre-edge peaks.

shift of the edge position to higher energy can be appreciated, passing from 7119.5 to 7123.0 eV. Simultaneously, in the pre-edge region, the component at 7112.3 eV is eroded in favor of a major peak at 7113.9 eV. At a more attentive look, it can be noted that the position of the pre-edge peak (7113.9 eV) does not exactly correspond to that of the sample oxidized by N_2O (7114.3 eV, see Figure 1 and Table 1), which in turn closely matched the position of the sample with template (vide supra). Additionally, the peak resulting from NO adsorption is considerably broader.

The outgassing at 573 K of the NO adsorbed on the sample (dashed curve in Figure 3) causes the partial erosion and a small blue-shift of the major pre-edge peak, which is now found at 7114.2 eV. Notwithstanding the asymmetry of the peak, the shoulder at 7112.3 eV is far from being restored, its intensity being now 0.067 (and not 0.098). Additionally, also the edge position is not totally restored after NO outgassing.

3.2. XANES Spectroscopy on Fe-MCM-22. A parallel series of experiments was performed on an Fe-MCM-22 sample with similar iron content but also incorporating Al framework species (Si/Fe = 44, Si/Al = 25). Figure 4 shows the effect of template removal and subsequent oxidation with N_2O on the MCM-22 sample under the experimental conditions that are the same as those in Figure 1 for Fe-silicalite. The spectrum of the sample with template (dashed curve) is very similar to that of Fe-silicalite (dashed line in Figure 1), indicating that practically all Fe is present as Fe^{3+} in an almost tetrahedral environment inside the framework.[51,52] Thermal activation causes a red-shift of the edge position (from 7124.2 to 7119.8 eV, see Table 1) comparable to that obtained on Fe-silicalite. The erosion of the pre-edge peak at 7114.2 eV, with the parallel increase of a new component around 7112.3 eV, is also very similar. We only observe a small difference in the relative intensity of two components observed in the Fe-silicalite and Fe-MCM-22 cases.

Upon oxidation, a shift of the edge position to higher energy and the modification of the pre-edge region (decrease of the component at 7112.3 eV, assigned to Fe^{2+} ions, and increase of the intensity of the peak at 7114.2 eV) are observed, in analogy to the Fe-silicalite case. However, while for Fe-silicalite the position of the edge after oxidation was almost coincident to that of the sample with template, in this case, the edge position is found halfway between the sample with template and the activated one. Coming to the EXAFS part of the X-ray absorption spectra (not reported for brevity), thermal activation at 1073 K causes a strong decrease of the intensity of the first Fe−O shell. The overall signal is very feeble so that it is not possible to discriminate if higher shells contributions are present. The oxidation with N_2O at 573 K causes a negligible modification of the EXAFS spectrum in the first shell region.

As already observed for the Fe-silicalite case, NO adsorption on the activated sample causes modifications in the edge position and in the pre-edge region of the XANES spectrum. More in detail, NO interaction with extraframework Fe ions causes the blue-shift of the edge position passing from 7119.8 to 7121.8 eV. The measured energy shift (2.0 eV, see Table 1) is sensibly lower than that obtained upon NO adsorption in the same conditions on Fe-silicalite (3.5 eV). In the pre-edge region, an increase of the pre-edge peak intensity, whose maximum position is now found at 7113.8 eV, is observed. As was already observed for Fe-silicalite, this new peak is broad and slightly asymmetric.

The subsequent degassing at 573 K brings back the spectrum to almost its original shape, with practically no difference from the spectra of the just activated sample (compare full and dashed line spectra in Figure 5).

3.3. UV−vis and FTIR Spectroscopy of Adsorbed NO on Fe-Silicalite and Fe-MCM-22. UV−vis spectroscopy was used to investigate the nature of iron on the thermally treated Fe-silicalite and Fe-MCM-22 samples (full and dotted curves, respectively in Figure 6). Both samples were previously activated at 1073 K. Both samples are characterized by an intense adsorption with an edge at 33 700 (Fe-silicalite) and 31 300 cm^{-1} (Fe-MCM-22). In Fe-silicalite, a broad tail (where at least two components centered around 27 000 and 21 000 cm^{-1} can be distinguished) is clearly visible in the 30 000−20 000 cm^{-1} range. In sample Fe-MCM-22, the tail of the edge adsorption is found in the same spectral range, with higher intensity.

TABLE 1: Position and Normalized Intensity of the 1s → 3d Pre-edge Peak of the XANES Spectra of Model Compounds, Fe-Silicalite and Fe-MCM-22, after Different Treatments[a]

	pre-edge peak		edge	edge shift
sample	position (eV)	intensity	position (eV)	|ΔeV|
$FePO_4$	7114.2	0.133	7124.1	
Fe_2O_3	7113.4 (s)	0.062	7123.9	
	7114.6	0.090		
$FeCp_2$	7112.4	0.064	7119.7	
Fe-MFI template	7114.2	0.164	7124.1	
Fe-MFI activated[b]	7112.3	0.066	7120.3	3.8[d]
	7114.2	0.083		
Fe-MFI oxidized	7114.3	0.128	7124.1	0[d]
Fe-MFI activated[c]	7112.3	0.098	7119.5	4.6[d]
	7114.2	0.115		
Fe-MFI + NO	7113.9	0.156	7123.0	3.5[e]
Fe-MFI + NO + outgas	7112.3 (s)	0.067	7121.4	1.9[e]
	7114.2	0.115		
Fe-MCM-22 template	7114.2	0.146	7124.2	
Fe-MCM-22 activated[b]	7112.3	0.053	7119.8	4.4[d]
	7114.2	0.064		
Fe-MCM-22 oxidized	7114.2	0.093	7122.3	1.9[d]
Fe-MCM-22 activated[c]	7112.4	0.055	7119.8	4.4[d]
	7114.1	0.065		
Fe-MCM-22 + NO	7113.8	0.116	7121.8	2.0[e]
Fe-MCM-22 +NO + outgas	7112.4	0.058	7120.0	0.2[e]
	7114.1	0.070		

[a] (s) = shoulder. The edge of the 1s → 3d peak of Fe metal foil (defined at the inflection point) has been set to 7111.6 eV. [b] Before oxidation. [c] Before NO dosage. [d] Shift with respect to the sample with template. [e] Shift with respect to the activated sample.

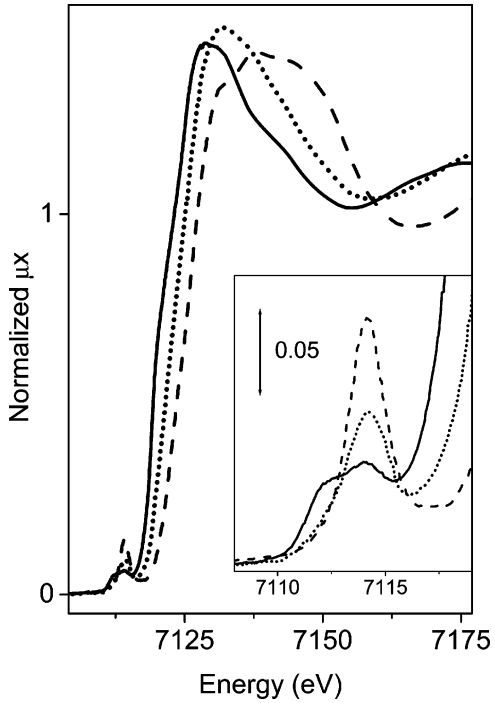

Figure 4. XANES spectra of sample Fe-MCM-22 with template (dashed line), after removal of template and subsequent activation at 1073 K (full line), and subsequent oxidation with N_2O at 523 K (dotted line). The inset shows the magnification of the pre-edge peaks.

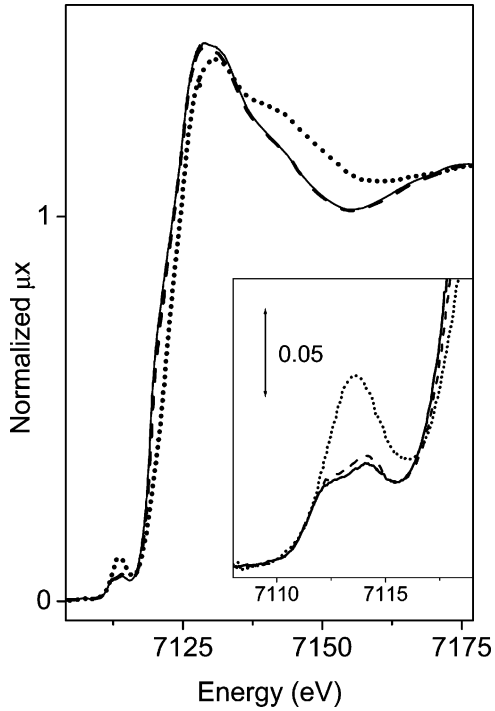

Figure 5. XANES spectra of sample Fe-MCM-22 after activation at 1073 K (full line), after dosage of 20 Torr NO at room temperature (dotted line), and subsequent outgassing at 573 K (dashed line). The inset shows the magnification of the pre-edge peaks.

The results obtained by FTIR spectroscopy upon varying NO equilibrium pressure (P_{NO}) at room temperature on samples Fe-silicalite and Fe-MCM-22, previously activated at 1073 K, are reported in Figure 7a and b, respectively. The intensity of IR nitrosyl bands was normalized with respect to the iron content of the samples crossed by the IR beam, as detailed in the Experimental Section. As a first observation, we underline the minor overall intensity of the nitrosyl bands obtained on Fe-MCM-22 sample with respect to Fe-silicalite one.

From a qualitative point of view, the nitrosyl bands obtained on the two samples show many analogies but also differences and will be described separately. On Fe-silicalite (Figure 7a), the high coverage spectrum (dashed curve) is composed by a major asymmetric band with a maximum at 1809 cm^{-1}, together with less intense but well-defined features in the 1925−1900 cm^{-1} interval, at 1875 cm^{-1} and at 1765 cm^{-1} (shoulder). By decreasing the P_{NO} (full lines), the intensity of all of these bands decreases, in favor of a pair at 1828 and 1759 cm^{-1}. The intensity of the latter couple increases, and they finally dominate

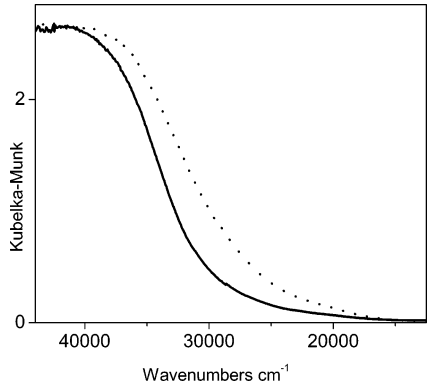

Figure 6. UV−vis spectra of samples Fe-silicalite (full line) and Fe-MCM-22 (dotted line) after thermal activation at 1073 K.

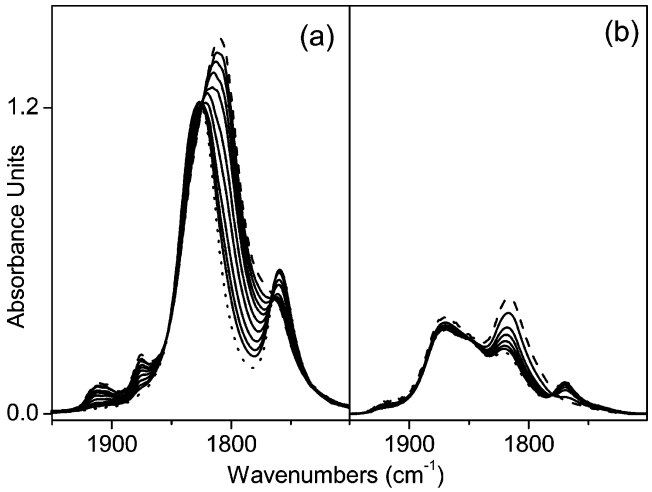

Figure 7. FTIR spectra of NO dosed at room temperature (decreasing P_{NO} from 15 Torr, dashed line spectrum to 10^{-3} Torr, dotted line spectrum) on (a) Fe-silicalite and (b) Fe-MCM-22 samples previously activated in vacuo at 1073 K. Spectra were normalized with respect to the pellet thickness and also with respect to the iron content as detailed in the Experimental Section.

the spectrum after prolonged outgassing at room temperature (dotted curve).

The spectra obtained upon NO dosage on Fe-MCM-22 (previously activated at 1073 K) are reported in Figure 7b. At high NO coverage, three main adsorptions dominate the spectrum (dashed line) with maxima at 1923, 1870, and 1825 cm^{-1}. Upon decreasing NO pressure, the intensity of these bands decreases in favor of two adsorptions at 1848 (shoulder) and 1769 cm^{-1}.

4. Discussion

4.1. XANES Spectroscopy on Fe-Silicalite. XANES spectroscopy has been widely employed in the determination of the oxidation states and of the local symmetries of Fe ions in different matrixes.[26,30,34,56,63−76] The pre-edge feature of the Fe K-edge adsorption spectrum arises from transitions of an Fe 1s electron into the lowest unoccupied electronic states, mainly having Fe 3d character. When the metal is found in a centrosymmetric environment, the 1s → 3d transitions are dipole forbidden, and thus show low intensity. However, a deviation from a centrosymmetric environment allows mixing of 3d and 4p orbitals. This hybridization plus a small dipole allowed 1s → 4p character to the 3d transitions, causing an enhancement of the pre-edge adsorption. As a consequence, changes in the pre-edge intensity reflect changes in the local environment of the metal ion, while the pre-edge position can be related to the oxidation state of Fe, in other words, to the occupation of the 3d band.[26,63−65,67,69]

The influence of the oxidation and coordination state of the metal center on XANES features has been deeply demonstrated by the systematic work of Wilke et al.,[67] where several Fe-containing minerals were analyzed. Unfortunately, the authors showed that the relation between oxidation state and the position of pre-edge features, Fe local symmetry, and pre-edge features intensity is far from linear. This lack of linearity forces the use of the quantitative analysis only when a couple of iron species are present, or when there is a clear knowledge of the structure of the involved iron species. Moreover, in this kind of analysis, a fundamental step, to estimate the intensity, is the background removal. This process requires a superlative signal-to-noise ratio, which is only obtainable increasing the amount of iron[30,72] or using Kβ detection. In fact, Battiston et al. were able to successfully apply quantitative analysis due to the higher concentration of iron,[30,72] while Heijboer et al. used it in samples with a less important Fe migration from framework position.[73]

For a correct interpretation of XANES data, and to allow an easy comparison with the other data present in the literature, spectra of model compounds (where the oxidation and coordination state of the metal ion is perfectly defined) are measured in the same experimental conditions.[26,63,64,69,77] In the present case, we have measured $FePO_4$, as an example of Fe^{3+} in tetrahedral-like coordination and α-Fe_2O_3 for Fe^{3+} in octahedral symmetry. $FeCp_2$ (Cp = cyclopentadienyl) has been chosen as an example of an Fe^{2+} compound. For the sake of comparison, both position and intensity of the 1s → 3d pre-edge peaks have been summarized in Table 1, while the corresponding spectra have been omitted for the sake of brevity.

As far as the spectra of Figure 1 are concerned, the decrease of the pre-edge peak intensity upon activation at 1073 K (passing from 0.16 to 0.08) can be explained with the migration of iron from a tetrahedral framework environment to an extraframework position.[26,65] The shift of the edge position and the appearance of the component at 7112.3 eV are interpreted as an $Fe^{3+} \rightarrow Fe^{2+}$ reduction accompanying the iron migration.[26,69] With respect to the XANES spectra previously published by us on similar Fe-silicalite[26,69] and Fe-MCM-22[56] samples, the quality improvement of the spectra is evident. We attribute this improvement to the higher activation temperature (1073 K vs 973 or 773 K) adopted in this study, which involves a larger extraframework migration. The evolution of the EXAFS spectra upon thermal activation (Figure 2) can be interpreted with the breaking of framework Fe−O bonds and the generation of a heterogeneous mixture of extraframework Fe ions with high static Debye−Waller factors that kill the EXAFS signal,[26,69] in good agreement with the previous picture.

The spectroscopic modifications caused by oxidation with N_2O at 523 K (shift of the edge position and changes in the intensities of the pre-edge components, vide supra) testify the reoxidation by N_2O of extraframework Fe^{2+} species, formed during activation, to Fe^{3+}. By comparing the spectrum of the oxidized sample with that of the sample with template, the following observations can be drawn. The edge positions of the two spectra are found at the same energy, and the same holds, within experimental uncertainty, for the maximum of the pre-edge peak. However, the spectral shape is totally different, and the intensity of the pre-edge peak, as well as its fwhm, does not reach the initial value. This is in agreement with the reoxidation of the previously reduced species, but definitely excludes the reintroduction of iron in the framework. Notice

that EXAFS data indicate an increase in the average coordination number of Fe sites after the oxidation. This suggests the presence of chemically adsorbed oxygen, coming from N_2O decomposition, in agreement with the observations of the Panov group on α-oxygen formation.[22,78]

The interaction between Fe sites in activated Fe-silicalite and NO molecules has been investigated by XANES spectroscopy, as shown in Figure 3 (dotted spectrum). This experiment is complementary to the well-known FTIR evidence that NO is a useful probe molecule to investigate the accessibility and coordinative unsaturation of extraframework iron ions, vide infra section 4.3. In fact, depending on the local environment, extraframework species can add up to 3 NO molecules, generating a mixture of $Fe^{3+}(NO)$, $Fe^{2+}(NO)$, $Fe^{2+}(NO)_2$, and $Fe^{2+}(NO)_3$ complexes.[25,26,32,33,56,79−81]

As anticipated above, the modifications of the XANES spectrum upon NO dosage are, at first sight, roughly similar to that observed after oxidation with N_2O. More in detail, the edge shift and the pre-edge modifications caused by NO suggest a formal oxidation of Fe^{2+}, previously reduced by thermal activation (vide supra), to Fe^{3+}. This could be explained by the formation of complexes, characterized by a strong metal to ligand charge transfer, which can be formalized as $Fe^{3+}(NO^-)$. This in turn would imply, on the basis of the simple molecular orbital theory, a bent NO geometry.[82] The broad character of the pre-edge peak obtained by NO adsorption can be explained in terms of the simultaneous presence of different nitrosyl complexes, in agreement with the complex IR spectroscopy described in the literature,[26,79,81] vide infra section 4.3. Upon outgassing of NO at 573 K, the XANES spectrum of the activated sample is not totally restored. The analogous experiment followed by FTIR spectroscopy (not reported) indicates that a thermal treatment at this temperature is able to totally desorb all nitrosyl complexes. This implies that the interaction of NO irreversibly modified the iron sites.

4.2. XANES Spectroscopy on Fe-MCM-22. The overall spectral modifications induced by thermal activation of Fe-MCM-22 sample, that is, the erosion of the pre-edge peak at 7114.2 eV, with the parallel increase of a new component around 7112.3 eV and the shift of the edge position to lower energy, are virtually identical to those observed for Fe-silicalite. These modifications are compatible with the migration of a fraction of Fe^{3+} framework sites to extraframework positions, with their concomitant reduction to Fe^{2+}. The modifications induced by N_2O oxidation (decrease of the component at 7112.3 eV, assigned to Fe^{2+} ions, and increase of the intensity of the peak at 7114.2 eV) are also qualitatively similar to the Fe-silicalite case.

From a quantitative point of view, the reoxidation of Fe-MCM-22 and Fe-silicalite samples is different, suggesting that, while the reoxidation process was complete for the Fe-silicalite case, only a fraction of previously reduced extraframework iron were reoxidized by N_2O in Fe-MCM-22. Due to the fact that the pre-edge features are not only sensitive to the oxidation state but also to the local environment of the metal ion, the interpretation of the changes is not straightforward. The fact that not all iron species are oxidized by N_2O could be explained in terms of aggregation of extraframework Fe species inside or outside the MCM-22 crystals during the thermal activation. This would imply a decrease of the amount of accessible and coordinatively unsaturated Fe ions. A second explanation could be related to the presence of Al atoms in the close vicinity of the extraframework Fe sites, influencing their electronic properties and thus their redox behavior.[34] A similar hypothesis was proposed to explain the different frequency of IR nitrosyl bands in Al-containing and Al-free Fe-MFI samples[32] and could be compatible with the FTIR spectroscopy of the same samples (vide infra). However, this hypothesis would not explain the similar shift of Al-free Fe-silicalite and Al-containing Fe-MCM-22 when Fe sites are reduced by thermal activation (vide supra and Table 1).

Coming to the EXAFS part of the X-ray absorption spectra, the overall evolution of the spectra is in good agreement with the XANES interpretation. In analogy with Fe-silicalite, thermal activation at 1073 K causes a strong decrease of the intensity of the first Fe−O shell, already interpreted with the breaking of framework Fe−O bonds and with the formation of new extraframework species characterized by a highly heterogeneous Fe−O distances distribution. EXAFS is usually a very sensitive technique to determine the presence of clustered species.[38] In the present case, due the low iron content of the sample and to the heterogeneity of the Fe sites, the EXAFS signal of the Fe-MCM-22 sample activated at 1073 K is very feeble. It is thus not possible to discriminate between noise and the contribution of a second shell. The oxidation with N_2O at 573 K causes a negligible modification of the EXAFS spectrum in the first shell region.

As was already observed for the Fe-silicalite case, NO adsorption on the activated Fe-MCM-22 sample causes modifications in the edge position and in the pre-edge region of the XANES spectrum, which are compatible with the change in the formal oxidation state of Fe^{2+} ions and with the formation of $Fe^{3+}(NO^-)$ complexes. The measured energy shift (2.0 eV, see Table 1) is considerably lower than that obtained upon NO adsorption in the same conditions on Fe-silicalite (3.5 eV). This fact is in agreement with the trend observed during oxidation of the MCM-22 sample, discussed above. In both cases, in fact, it appears that only a part of the extraframework Fe sites is sensitive to reactants.

The subsequent degassing of NO at 573 K brings back the spectrum to almost its original shape, with practically no difference from the spectrum of the just activated sample (compare full and dashed line spectra in Figure 5). This could be interpreted as a different reducibility of extraframework Fe sites as a consequence of the presence of Al,[34] resulting in a total reversibility of the NO interaction. However, it seems more likely that XANES spectroscopy is not able to appreciate a partial irreversibility on a minor fraction of Fe species (those accessible to ligands). IR investigations will further support this interpretation.

4.3. UV−vis and FTIR Spectroscopy of Adsorbed NO on Fe-Silicalite and Fe-MCM-22. UV−vis spectroscopy is usually employed to investigate the nature of Fe sites in siliceous matrixes.[11,65,69,83] In analogy with XAFS spectroscopies, UV−vis is an average technique, and the adsorptions due to isolated and clustered, reduced and oxidized species are often superimposed. Moreover, UV−vis adsorptions are usually very broad, so that it is generally hard to gain detailed information about systems where a heterogeneous distribution of Fe sites is present. However, this technique can be employed to obtain average information about the presence of iron oxide clusters, and at this scope it was used in this study.

The spectra of thermally activated Fe-silicalite and Fe-MCM-22 samples (full and dotted curves, respectively, in Figure 6) show an intense adsorption with ligand to metal charge-transfer (CT) character, easily assigned to O → Fe CT transitions. It has been shown that the edge position of the O → Fe CT adsorption can be used to estimate the clustering degree of Fe

ions.[11,83] For example, isomorphously substituted Fe-zeolites before thermal treatments are characterized by a strong CT absorption with the edge position around 38 000 cm^{-1}, assigned to O → Fe CT transitions involving isolated Fe^{3+} in framework tetrahedral positions.[83] The red-shift of the edge position in thermally treated samples has been explained with progressive clustering of the extraframework Fe ions.

A detailed analysis of the UV−vis spectroscopy for the determination of nuclearity and structure of the Fe_xO_y clusters is seriously challenging and outside the scope of this paper. Instead, a qualitative comparison of the spectra obtained on the two samples can be made. The spectrum obtained on Fe-MCM-22 sample shows a consistent red-shift of the CT band with respect to Fe-silicalite. Moreover, the intensity in the 30 000−20 000 cm^{-1} range, typically assigned to small oligonuclear clusters, is higher in former samples. These features are consistent with a larger clustering process in Fe-MCM-22, in agreement with XANES data and with IR spectra (see below).

The nature of iron species in Fe-containing zeolites samples is frequently investigated by FTIR spectroscopy using NO as probe molecule. This technique was successfully used by several groups[25,26,32,41,56,66,79,81,84,85] to characterize the exposed sites of different iron-containing molecular sieves, and it is based on the capability of low coordinated Fe^{2+} and Fe^{3+} ions to form stable NO adducts ($Fe(NO)_n$, $n = 1, 2, 3$) at room temperature. The maximum number of NO ligands adsorbed by each Fe^{2+} and Fe^{3+} center represents a direct indication of their coordinative unsaturation and allows one to differentiate the exposed Fe species, that is, extraframework Fe^{2+} and Fe^{3+} ions in isolated positions, in small extraframework clusters (like dinuclear ones) or present at the surface of bigger particles.[26] Due to the high IR extinction coefficient of the $Fe(NO)_n$ complexes, even samples containing very low Fe content could be investigated.[32] From what has been stated above, the IR spectroscopy of the NO probe allows the detailed exploration of all of the accessible Fe surface sites, while Fe sites not located in surface positions (and hence surely not active, such as bulk atoms in Fe_xO_y particles) escape this probing procedure.

The results obtained by FTIR spectroscopy upon varying NO equilibrium pressure (P_{NO}) at room temperature on samples Fe-silicalite and Fe-MCM-22, previously activated at 1073 K, are reported in Figure 7a and b, respectively. As a first observation, we underline the minor overall intensity of the nitrosyl bands obtained on Fe-MCM-22 sample with respect to the Fe-silicalite one. This trend is in agreement with the XANES evidence that only a fraction of the extraframework Fe sites in Fe-MCM-22 is able to interact with NO (vide supra Figures 3 and 5, confirming the cluster already observed by UV−vis (see Figure 6).

The nitrosyl bands obtained upon NO dosage on Fe-silicalite activated at 1073 K (Figure 7a) are complex, so that comparison with other known systems was necessary for their interpretation, as was deeply discussed elsewhere.[25,33] The assignment of the complex spectroscopy has been separated into two independent groups of adsorptions. Coming to the first group, the transformation of the couple of bands at 1809 and 1912 cm^{-1} into a pair growing around 1828 and 1759 cm^{-1} upon decreasing P_{NO} has been often observed in Fe-zeolites and has been explained with an $Fe^{2+}(NO)_3 \rightleftharpoons Fe^{2+}(NO)_2$ equilibrium.[26,84] This assignment, testified by the presence of three isosbestic points at 1853, 1825, and 1766 cm^{-1}, was confirmed by an experiment performed with a 1:1 $^{14}NO/^{15}NO$ isotopic mixture.[84] Notice that in the present case the bands at 1912 and 1809 cm^{-1} are broad and asymmetric, testifying the presence of a complex family of slightly different Fe^{2+} sites with slightly different local environments, which depend on the location of iron inside the zeolitic channels.[26]

Coming to the second group of adsorptions, an additional sharp peak, not explainable with the previous equilibrium, is clearly observed at 1875 cm^{-1}. The intensity of this peak decreases with P_{NO} and could be correlated to the decrease of a component of the main 1809 cm^{-1} band (shoulder at 1776 cm^{-1}). This feature was only observed on Fe-silicalite after activation at high temperature (1073 K) and could be explained by comparison with the samples prepared by anchoring Fe to amorphous matrixes (silica or mesoporous MCM-41).[25,33] The presence of the minor feature at 1875 cm^{-1} is testifying the formation of a family of "amorphous-like" Fe^{2+} sites, able to add only 2 NO molecules. The formation of those Fe sites was explained by assuming a local amorphization of the zeolitic framework as a consequence of high-temperature treatments. These Fe ions show a lower coordinative unsaturation with respect to the Fe^{2+} ions able to add 3 NO ligands, suggesting a strong effect of the zeolitic framework in the Fe site coordination.

The spectra obtained upon NO dosage on Fe-MCM-22 (previously activated at 1073 K) are reported in Figure 7b. By analogy with that already observed in Fe-MFI samples, we assign the evolution of the couple of bands at 1923/1815 into the 1848/1769 cm^{-1} pair to the $Fe^{2+}(NO)_3 \rightleftharpoons Fe^{2+}(NO)_2$ equilibrium. Notice that the position of the corresponding bands is blue-shifted with respect to that observed in Fe-silicalite. This observation is in agreement with the presence of Al in the MCM-22 framework and was already observed by comparing Al-free Fe-silicalite with Fe-ZSM-5 samples.[32] The broad and asymmetric adsorption at 1870 cm^{-1} can be ascribed to the formation of mononitrosyl complexes formed with Fe ions on the surface of clustered species. Notice that the spectroscopic features ascribed to a family of "amorphous-like" Fe^{2+} sites, able to add only 2 NO molecules, are not observed on the Al-containing Fe-MCM-22 sample treated at high temperature, indicating a higher stability of the framework.

5. Conclusions

In situ XANES spectroscopy has been used to investigate the modification of the oxidation and coordination states of Fe species, hosted inside MFI and MCM-22 framework, upon template burning, N_2O oxidation, and NO coordination. Parallel experiments, regarding NO coordination, have been performed with IR spectroscopy also. With respect to previous studies,[26,56,69] for both Fe-MFI and Fe-MCM-22 samples, the higher activation temperature adopted here (1073 K) caused an almost complete migration of framework Fe^{3+} species into extraframework Fe^{2+}; consequently, the XANES feature of the latter species has been much better resolved. The two samples exhibit a different behavior when the interaction with molecules is investigated, which is due to the different ratio between the isolated and clustered Fe species formed after the thermal activation.

Upon oxidation with N_2O at 523 K, in Fe-silicalite practically all of the Fe^{2+} sites formed by thermal activation are reoxidized to Fe^{3+}, while in Fe-MCM-22 only a fraction of the extraframework iron sites is involved in the reoxidation process.

Upon NO dosage on the Fe-silicalite sample, the modification of the pre-edge peak and of the edge position suggests an important charge release from the extraframework Fe^{2+} ions to the adsorbed molecules. This could be formalized with the formation of $Fe^{3+}(NO^-)$ complexes, compatible with a bent NO

geometry. The formation of a complex family of Fe^{2+} mono-, di-, and trinitrosyl complexes was also confirmed by FTIR spectroscopy. Similarly to what was observed in the oxidation experiments, the fraction of extraframework Fe sites able to interact with NO in Fe-MCM-22 sample is smaller than that in Fe-silicalite treated in the same conditions. This trend is explained with a major clustering of extraframework Fe sites in Fe-MCM-22 sample, as was also suggested by FTIR experiments.

Acknowledgment. We are indebted to the colleagues of Milano University (L. Forni) and of Calabria University (R. Aiello and F. Testa) for fruitful discussions and for the synthesis of Fe-silicalite and Fe-MCM-22 samples, respectively. We thank F. D'Acapito and all of the GILDA BM8 staff at the ESRF, where X-ray absorption measurements were carried out, and G. Ricchiardi for precious comments.

References and Notes

(1) Garten, R. L.; Delgass, W. N.; Boudart, M. *J. Catal.* **1970**, *18*, 90.
(2) Aparicio, L. M.; Hall, W. K.; Fang, S.-M.; Ulla, M. A.; Millman, W. S.; Dumesic, J. A. *J. Catal.* **1987**, *108*, 233.
(3) Szostak, R.; Thomas, T. L. *J. Catal.* **1986**, *100*, 555.
(4) Ratnasamy, P.; Kumar, R. *Catal. Lett.* **1993**, *22*, 227.
(5) Kharitonov, A. S.; Sheveleva, G. A.; Panov, G. I.; Sobolev, V. I.; Paukshtis, Y. A.; Romannikov, V. N. *Appl. Catal., A* **1993**, *98*, 33.
(6) Kikuchi, E.; Yogo, K.; Tanaka, S.; Abe, M. *Chem. Lett.* **1991**, 1063.
(7) Feng, X. B.; Hall, W. K. *J. Catal.* **1997**, *166*, 368.
(8) Ma, A. Z.; Grünert, W. *Chem. Commun.* **1999**, 71.
(9) Roy, P. K.; Pirngruber, G. D. *J. Catal.* **2004**, *227*, 164.
(10) Pirngruber, G. D. *J. Catal.* **2003**, *219*, 456.
(11) Pérez-Ramírez, J.; Kumar, M. S.; Brückner, A. *J. Catal.* **2004**, *223*, 13.
(12) Brosius, R.; Habermacher, D.; Martens, J. A.; Vradman, L.; Herskowitz, M.; Capek, L.; Sobalík, Z.; Dědeček, J.; Wichterlová, B.; Tokarová, V.; Gonsiorová, O. *Top. Catal.* **2004**, *30*−*31*, 333.
(13) Zhu, Q.; Mojet, B. L.; Janssen, R. A. J.; Hensen, E. J. M.; van Grondelle, J.; Magusin, P.; van Santen, R. A. *Catal. Lett.* **2002**, *81*, 205.
(14) El-Malki, E. M.; van Santen, R. A.; Sachtler, W. M. H. *J. Catal.* **2000**, *196*, 212.
(15) Choi, S. H.; Wood, B. R.; Ryder, J. A.; Bell, A. T. *J. Phys. Chem. B* **2003**, *107*, 11843.
(16) Ryder, J. A.; Chakraborty, A. K.; Bell, A. T. *J. Catal.* **2003**, *220*, 84.
(17) Liang, J.; Zhang, Q. H.; Wu, H. L.; Meng, G. Y.; Tang, Q. H.; Wang, Y. *Catal. Commun.* **2004**, *5*, 665.
(18) Pillai, K. S.; Jia, J. F.; Sachtler, W. M. H. *Appl. Catal., A* **2004**, *264*, 133.
(19) Jia, J. F.; Pillai, K. S.; Sachtler, W. M. H. *J. Catal.* **2004**, *221*, 119.
(20) Fejes, P.; Lazar, K.; Marsi, I.; Rockenbauer, A.; Korecz, L.; Nagy, J. B.; Perathoner, S.; Centi, G. *Appl. Catal., A* **2003**, *252*, 75.
(21) Fejes, P.; Kiricsi, I.; Lazar, K.; Marsi, I.; Rockenbauer, A.; Korecz, L.; Nagy, J. B.; Aiello, R.; Testa, F. *Appl. Catal., A* **2003**, *242*, 247.
(22) Dubkov, K. A.; Ovanesyan, N. S.; Shteinman, A. A.; Starokon, E. V.; Panov, G. I. *J. Catal.* **2002**, *207*, 341.
(23) Faggian, S.; Fisicaro, P.; Giamello, E.; Gobetto, R.; Viale, A.; Berlier, G.; Lamberti, C.; Rossetti, I. *J. Phys. Chem. B* **2003**, *107*, 8922.
(24) Marturano, P.; Drozdova, L.; Kogelbauer, A.; Prins, R. *J. Catal.* **2000**, *192*, 236.Marturano, P.; Drozdova, L.; Pirngruber, G. D.; Kogelbauer, A.; Prins, R. *Phys. Chem. Chem. Phys.* **2001**, *3*, 5585.
(25) Berlier, G.; Bonino, F.; Zecchina, A.; Bordiga, S.; Lamberti, C. *ChemPhysChem* **2003**, *4*, 1073.
(26) Berlier, G.; Spoto, G.; Bordiga, S.; Ricchiardi, G.; Fisicaro, P.; Zecchina, A.; Rossetti, I.; Selli, E.; Forni, L.; Giamello, E.; Lamberti, C. *J. Catal.* **2002**, *208*, 64.
(27) Pirngruber, G. D.; Luechinger, M.; Roy, P. K.; Cecchetto, A.; Smirniotis, P. *J. Catal.* **2004**, *224*, 429.
(28) Battiston, A. A.; Bitter, J. H.; Koningsberger, D. C. *Catal. Lett.* **2000**, *66*, 75.
(29) Battiston, A. A.; Bitter, J. H.; Koningsberger, D. C. *J. Catal.* **2003**, *218*, 163.
(30) Battiston, A. A.; Bitter, J. H.; Heijboer, W. M.; de Groot, F. M. F.; Koningsberger, D. C. *J. Catal.* **2003**, *215*, 279.
(31) Pirutko, L. V.; Chernyavsky, V. S.; Uriarte, A. K.; Panov, G. I. *Appl. Catal., A* **2002**, *227*, 143.
(32) Berlier, G.; Zecchina, A.; Spoto, G.; Ricchiardi, G.; Bordiga, S.; Lamberti, C. *J. Catal.* **2003**, *215*, 264.
(33) Berlier, G.; Ricchiardi, G.; Bordiga, S.; Zecchina, A. *J. Catal.* **2005**, *229*, 127.
(34) Hensen, E.; Zhu, Q. J.; Liu, P. H.; Chao, K. J.; van Santen, R. *J. Catal.* **2004**, *226*, 466.
(35) Hensen, E. J. M.; Zhu, Q.; van Santen, R. A. *J. Catal.* **2003**, *220*, 260.
(36) Choi, S. H.; Wood, B. R.; Bell, A. T.; Janicke, M. T.; Ott, K. C. *J. Phys. Chem. B* **2004**, *108*, 8970.
(37) Wichterlová, B.; Sobalík, Z.; Dědeček, J. *Appl. Catal., B* **2003**, *41*, 97.
(38) Ferretti, A. M.; Oliva, C.; Forni, L.; Berlier, G.; Zecchina, A.; Lamberti, C. *J. Catal.* **2002**, *208*, 83.
(39) Centi, G.; Genovese, C.; Giordano, G.; Katovic, A.; Perathoner, S. *Catal. Today* **2004**, *91*−*92*, 17.
(40) Chen, H. Y.; Wang, X.; Sachtler, W. M. H. *Appl. Catal., A* **2000**, *194*, 159.
(41) Mul, G.; Zandbergen, M. W.; Kapteijn, F.; Moulijn, J. A.; Pérez-Ramírez, J. *Catal. Lett.* **2004**, *93*, 113.
(42) Nobukawa, T.; Yoshida, M.; Kameoka, S.; Ito, S. I.; Tomishige, K.; Kunimori, K. *Catal. Today* **2004**, *93*−*95*, 791.
(43) Pérez-Ramírez, J.; Gallardo-Llamas, A. *J. Catal.* **2004**, *223*, 382.
(44) Novakova, J.; Schwarze, M.; Tvaruzkova, Z.; Sobalik, Z. *Catal. Lett.* **2004**, *98*, 123.
(45) Giles, R.; Cant, N. W.; Kogel, M.; Turek, T.; Trimm, D. L. *Appl. Catal., B* **2000**, *25*, L75.
(46) Long, R. Q.; Yang, R. T. *J. Catal.* **2002**, *207*, 274.
(47) Stockenhuber, M.; Joyner, R. W.; Dixon, J. M.; Hudson, M. J.; Grubert, G. *Microporous Mesoporous Mater.* **2001**, *44*, 367.
(48) Grubert, G.; Hudson, M. J.; Joyner, R. W.; Stockenhuber, M. *J. Catal.* **2000**, *196*, 126.
(49) Lazar, K.; Fejes, P.; Pal-Borbely, G.; Beyer, A. K. *Hyperfine Interact.* **2002**, *141*, 387.
(50) Long, R. Q.; Yang, R. T. *J. Catal.* **1999**, *188*, 332.
(51) Wu, P.; Lin, H.; Komatsu, T.; Yashima, T. *Chem. Commun.* **1997**, 663.
(52) Testa, F.; Crea, F.; Diodati, G. D.; Pasqua, L.; Aiello, R.; Terwagne, G.; Lentz, P.; Nagy, J. B. *Microporous Mesoporous Mater.* **1999**, *30*, 187.
(53) Meloni, D.; Monaci, R.; Rombi, E.; Guimon, C.; Martinez, H.; Fechete, I.; Dumitriu, E. *Stud. Surf. Sci. Catal.* **2002**, *142*, 167.
(54) Wang, Y.; Yang, G.; Zhou, D. H.; Bao, X. H. *J. Phys. Chem. B* **2004**, *108*, 18228.
(55) Wang, Y.; Zhou, D. H.; Yang, G.; Miao, S. J.; Liu, X. C.; Bao, X. H. *J. Phys. Chem. A* **2004**, *108*, 6730.
(56) Berlier, G.; Pourny, M.; Bordiga, S.; Spoto, G.; Zecchina, A.; Lamberti, C. *J. Catal.* **2005**, *229*, 45.
(57) Leonowicz, M. E.; Lawton, J. A.; Lawton, S. L.; Rubin, M. K. *Science* **1994**, *264*, 1910.
(58) Corma, A.; Corell, C.; PerezPariente, J.; Guil, J. M.; GuilLopez, R.; Nicolopoulos, S.; Calbet, J. G.; ValletRegi, M. *Zeolites* **1996**, *16*, 7.
(59) Ratnasamy, P.; Kumar, R. *Catal. Today* **1991**, *9*, 329.
(60) Pascarelli, S.; Boscherini, F.; Dacaptito, F.; Hrdy, J.; Meneghini, C.; Mobilio, S. *J. Synchrotron Radiat.* **1996**, *3*, 147.
(61) Lamberti, C.; Bordiga, S.; Bonino, F.; Prestipino, C.; Berlier, G.; Capello, L.; D'Acapito, F.; Xamena, F.; Zecchina, A. *Phys. Chem. Chem. Phys.* **2003**, *5*, 4502.
(62) Lamberti, C.; Prestipino, C.; Bordiga, S.; Berlier, G.; Spoto, G.; Zecchina, A.; Laloni, A.; La Manna, F.; D'Anca, F.; Felici, R.; D'Acapito, F.; Roy, P. *Nucl. Instrum. Methods Phys. Res., Sect. B* **2003**, *200*, 196.
(63) Bordiga, S.; Geobaldo, F.; Lamberti, C.; Zecchina, A.; Boscherini, F.; Genoni, F.; Leofanti, G.; Petrini, G.; Padovan, M.; Geremia, S.; Vlaic, G. *Nucl. Instrum. Methods Phys. Res., Sect. B* **1995**, *97*, 23.
(64) Westre, T. E.; Kennepohl, P.; DeWitt, J. G.; Hedman, B.; Hodgson, K. O.; Solomon, E. I. *J. Am. Chem. Soc.* **1997**, *119*, 6297.
(65) Bordiga, S.; Buzzoni, R.; Geobaldo, F.; Lamberti, C.; Giamello, E.; Zecchina, A.; Leofanti, G.; Petrini, G.; Tozzola, G.; Vlaic, G. *J. Catal.* **1996**, *158*, 486.
(66) Chen, H. Y.; El-Malki, E. M.; Wang, X.; van Santen, R. A.; Sachtler, W. M. H. *J. Mol. Catal. A* **2000**, *162*, 159.
(67) Wilke, M.; Farges, F.; Petit, P. E.; Brown, G. E.; Martin, F. *Am. Mineral.* **2001**, *86*, 714.
(68) Petit, P. E.; Farges, F.; Wilke, M.; Sole, V. A. *J. Synchrotron Radiat.* **2001**, *8*, 952.
(69) Berlier, G.; Spoto, G.; Fisicaro, P.; Bordiga, S.; Zecchina, A.; Giamello, E.; Lamberti, C. *Microchem. J.* **2002**, *71*, 101.
(70) Jia, J. F.; Sun, Q.; Wen, B.; Chen, L. X.; Sachtler, W. M. H. *Catal. Lett.* **2002**, *82*, 7.
(71) Heijboer, W. M.; Battiston, A. A.; Knop-Gericke, A.; Havecker, M.; Mayer, R.; Bluhm, H.; Schlögl, R.; Weckhuysen, B. M.; Koningsberger, D. C.; de Groot, F. M. F. *J. Phys. Chem. B* **2003**, *107*, 13069.

(72) Battiston, A. A.; Bitter, J. H.; de Groot, F. M. F.; Overweg, A. R.; Stephan, O.; van Bokhoven, J. A.; Kooyman, P. J.; van der Spek, C.; Vanko, G.; Koningsberger, D. C. *J. Catal.* **2003**, *213*, 251.

(73) Heijboer, W. M.; Glatzel, P.; Sawant, K. R.; Lobo, R. F.; Bergmann, U.; Barrea, R. A.; Koningsberger, D. C.; Weckhuysen, B. M.; de Groot, F. M. F. *J. Phys. Chem. B* **2004**, *108*, 10002.

(74) Aitken, J. B.; Thomas, S. E.; Stocker, R.; Thomas, S. R.; Takikawa, O.; Armstrong, R. S.; Lay, P. A. *Biochemistry* **2004**, *43*, 4892.

(75) Rich, A. M.; Ellis, P. J.; Tennant, L.; Wright, P. E.; Armstrong, R. S.; Lay, P. A. *Biochemistry* **1999**, *38*, 16491.

(76) Pirngruber, G. D.; Roy, P. K.; Weiher, N. *J. Phys. Chem. B* **2004**, *108*, 13746.

(77) Bianconi, A. In *X-ray Absorption*; Koningsberger, D. C., Prins, R., Eds.; Wiley: New York, 1988; p 573.

(78) Starokon, E. V.; Dubkov, K. A.; Pirutko, L. V.; Panov, G. I. *Top. Catal.* **2003**, *23*, 137.

(79) Mul, G.; Pérez-Ramírez, J.; Kapteijn, F.; Moulijn, J. A. *Catal. Lett.* **2002**, *80*, 129.

(80) Krishna, K.; Seijger, G. B. F.; van den Bleek, C. M.; Makkee, M.; Mul, G.; Calis, H. P. A. *Catal. Lett.* **2003**, *86*, 121.

(81) Lobree, L. J.; Hwang, I. C.; Reimer, J. A.; Bell, A. T. *J. Catal.* **1999**, *186*, 242.

(82) Hawker, P. N.; Twigg, M. V. Iron(II) and lower states. In *Comprehensive Coordination Chemistry: The Synthesis, Reactions, Properties and Applications of Coordination Compounds*; Wilkinson, G., Gillard, R. D., McCleverty, J. A., Eds.; Pergamon: Oxford, 1987; p 1179.

(83) Bordiga, S.; Scarano, D.; Lamberti, C.; Zecchina, A.; Geobaldo, F.; Vlaic, G.; Buzzoni, R.; Tozzola, G.; Petrini, G. *J. Phys. IV* **1997**, *7*, 907.

(84) Spoto, G.; Zecchina, A.; Berlier, G.; Bordiga, S.; Clerici, M. G.; Basini, L. *J. Mol. Catal. A* **2000**, *158*, 107.

(85) Lezcano, M.; Kovalchuk, V. I.; d'Itri, J. L. *Kinet. Catal.* **2001**, *42*, 104.